

# Rare metals bearing pegmatites in the Nubian Shield: A case study of Ras Al-Baroud area, Eastern Desert of Egypt



Marian J. Matta<sup>1</sup>, Mokhles K. Azer<sup>2</sup> and Mahmoud H. Darwish<sup>1\*</sup>

<sup>1</sup> Geology Department, Faculty of Science, New Valley University, El-Kharga, 72511 Egypt

<sup>2</sup> Geological Sciences Department, National Research Centre, 12622 Dokki, Cairo, Egypt

Doi: [10.21608/nujbas.2024.259338.1020](https://doi.org/10.21608/nujbas.2024.259338.1020)

## Abstract

This study documents the geochemical evolution of rare-metal mineralized granitic pegmatite of Ras Al-Baroud using mineral chemistry and whole rock chemistry. Pegmatite occurs as sheet-like bodies, pockets along the edges of the Ras Al-Baroud post-collisional granite, or within fault zones. Pegmatites at the outer margins of Ras Al-Baroud granites show gradational boundaries. In a few outcrops, the Ras Al-Baroud pegmatites are affected by intense metasomatic-hydrothermal alteration resulting in albitization and greisenization: especially close to contact with the host rocks. Nb-Ta oxides are the most important rare metals in the Ras Al-Baroud pegmatite and are represented mainly by columbite and less amount of tantalite. They are commonly zoned, exhibiting a wide range of chemical compositions and are characterized by partial digestion and late-stage overgrowth due to the effecting of magmatic and hydrothermal processes in the granite-pegmatite system. Ras Al-Baroud pegmatite is considered to mainly crystallize late from a pegmatite-forming melt that resulted from a combination of magmatic and hydrothermal processes. Extended fractional crystallization in Ras Al-Baroud granites eventually produced saturated, late-magmatic fluids. These fluids migrated towards the apex of the magma chamber, reacting with still-hot but subsolidus granite and becoming increasingly focused into distinct channels and veins. This upward and outward mode of fluid migration led to pegmatites with gradational boundaries.

**Keywords:** Eastern Desert, Rare-metal granitic pegmatites, Muscovite; Columbite-group minerals, magmatic-hydrothermal evolution.

## Introduction

Granitic pegmatites represent highly evolved end members of granitic magmas. Therefore, the study of granitic pegmatites is essential for understanding the processes controlling magma evolution and the geochemical behavior of some rare metal elements. In addition, granitic pegmatites represent economically valuable rare-metal-bearing rocks and major sources of some strategic elements (e.g., Li, Be, B, Sn, Rb, Cs, Zr, Ta, and Nb). In this context, it is important to understand the role of the magmatic-hydrothermal process which affects during rare metal mineralization of the pegmatites. In general, rare-metal enrichment in the granitic pegmatites is usually influenced by fractional and hydrothermal processes [1-4].

The granitoid rocks and associated pegmatites are widely distributed in the Arabian-Nubian Shield (ANS) displaying complex petrological and geochemical signatures [5]. The ANS as a part of the Pan-African orogenic belt was initiated as an intra-oceanic island arc that underwent obduction-

accretion processes through the Neoproterozoic (e.g. [6]). The ANS is a geological complex that spans across parts of Northeast Africa and the Arabian Peninsula. It's a significant region known for its rich mineral deposits and complex geological history, covering areas of modern-day Saudi Arabia, Egypt, Sudan, Eritrea, Ethiopia, and Jordan. The granitoid rocks of the ANS include medium-K calc-alkaline, high-K calc-alkaline, strongly peraluminous, and A-type granites. They were formed in different tectonic settings and have different ages (e.g. [7-13]).

Recent scientific studies have shown the importance of strategic metals in many of the most important strategic and electronic industries of our time, which are indispensable for mankind. In Egypt, some rocks are known to have high concentrations of many of the strategic metals, especially the post-collisional granites and pegmatites [13-15]. However, despite the clear evidence of the presence of these metals in some granite plutons and associated pegmatites, assessment and understanding of genetic processes

remain poorly understood, due in part to the scarcity of research tools needed for exploration and evaluation.

The present work deals with granitic pegmatites in Ras Al-Baroud area, which is located in the north Eastern Desert of Egypt. These pegmatites are distributed in or around the granitoids in the Ras Al-Baroud granitic intrusion. The granitic rocks of Ras Al-Baroud intrusion are studied in detail by [Abuamarah \*et al.\*, \[13\]](#). In this study, we combine field works, petrography, mineral chemistry, and geochemistry of Ras Al-Baroud pegmatite to constrain internal geochemical evolution processes related to rare metal mineralization.

### Geological setting

The late Neoproterozoic basement rock units in the Eastern Desert of Egypt are dominated by gneiss domes, ophiolitic-related assemblages, island-arc metavolcanics and their derivative volcanoclastics. These rock units were episodically intruded by suites of syn-late to post-tectonic ultrabasic-basic and granitoid intrusions and intruded by post tectonic dykes and intraplate granites. Most of the granitic rocks of the ANS are associated with pegmatites.

Wadi Al-Baroud area, the target of the present work, is located in the north Eastern Desert of Egypt, close to the tectonic boundary with the Central Eastern Desert, ~ 35 km southwest of Safaga City ([Fig. 1](#)). It is dissected by several faults and structurally controlled wadis. The study area is located between latitudes 26° 43' & 26° 50' N and longitudes 33° 34' & 34° 44' E. The Neoproterozoic rock units cropping out in mapped area include syntectonic granitoids (granodiorite and tonalite), gabbros and post-collisional granites ([Fig. 2](#)). The relationships between the pegmatite and different rock units in the study area are indicated schematically in a NE-SW cross-section ([Fig. 3](#)). The granodiorite is the most common rock type in the mapped area and forms low to moderate reliefs. It is characterized by spheroidal weathering and contains microgranular mafic enclaves. Gabbro exposes at southeastern part of the study area that intruded the syntectonic granitoids with sharp intrusive contacts. The post-collisional granites form two isolated plutons separated by Wadi Al-Baroud. The most characteristic feature of the post-collisional granites is the absence of mafic enclaves and rare of dykes. They send offshoots and apophyses to the syntectonic granitoids along the contacts.

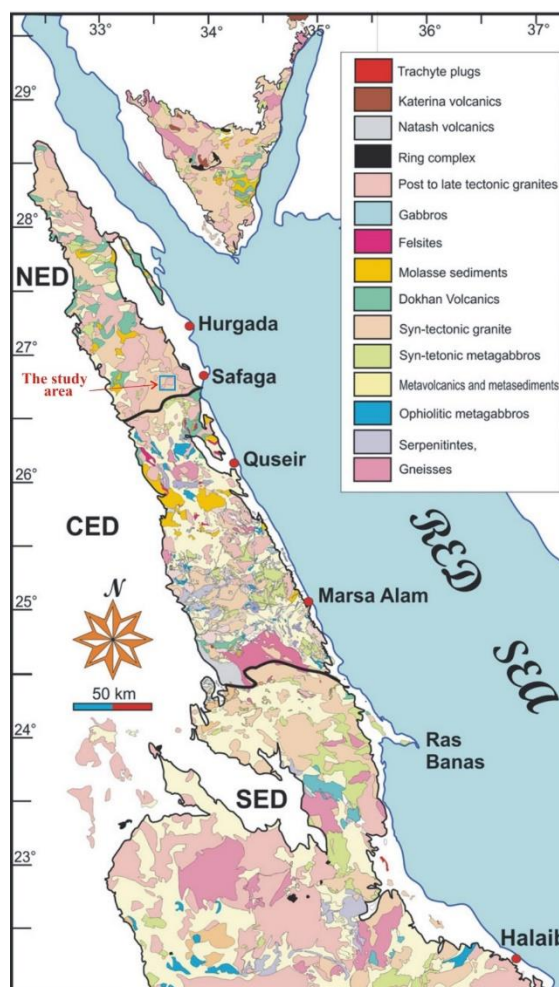


**Fig. 1.** Geological map of the Egyptian Nubian Shield showing three tectono-lithologic domains in the Eastern Desert (after [Abd El-Wahed and Hamimi, 2021\[14\]](#)) and the location of the study area is indicated.

Coarse-grained pegmatite is observed associated with the post-collisional granite as plugs and dikes ([Fig. 4](#)) that occur inside the pluton and along its peripheries and marginal parts. They show sharp contacts with their host rocks and are variable in their shapes and size. The granitic pegmatites in the study area are coarse-grained and show sequence of zones including microcline pegmatite, microcline albite pegmatite, and albite pegmatite. Rare-metals mineralized pegmatites mostly occur as dikes and lenticular bodies, several centimeters to several meters in width and in length. Some miarolitic cavities are found within the pegmatites. In few outcrops, the Ras Al-Baroud pegmatites are commonly affected by intense metasomatic-hydrothermal alteration resulting in albitization and greisenization; especially close to the contact with the host rocks.

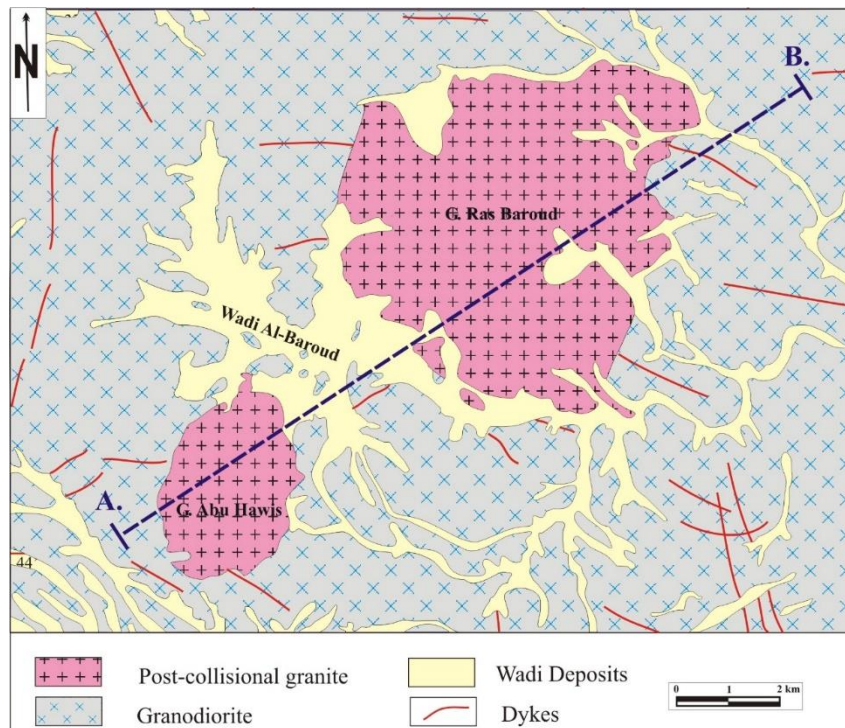


**Fig. 2.** The geologic map of the Wadi Al-Baroud area, modified after [Abuamarah et al., \[13\]](#) and the location of the cross-section (Fig. 3) is indicated.

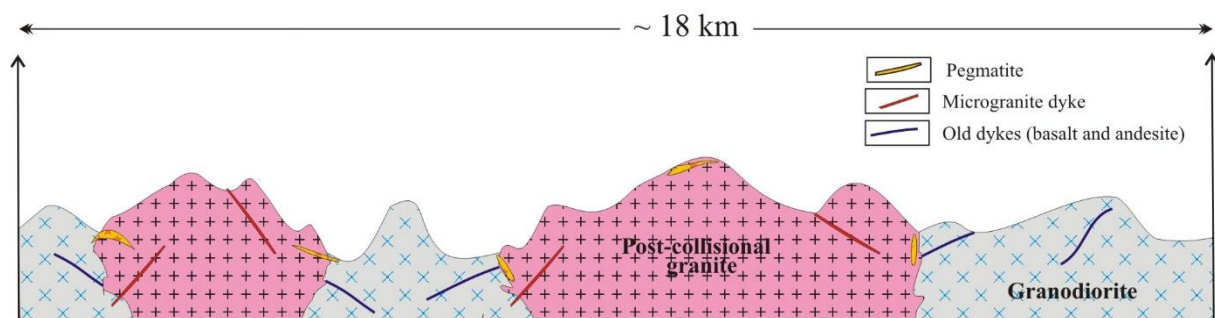


**Fig. 3.** Schematic geological cross-section showing the inferred relationships between the pegmatites and post-collisional granites in Wadi Al-Baroud.



**Fig. 4.** Pocket of pegmatite at the margin of Gebel Ras Al-Baroud granite

## Petrography

The pegmatites that are associated with the post-collisional granites in Ras Al-Baroud area show variable colors, grain sizes, textures, and mineral compositions. Based on the color and mineralogical composition, they can be distinguished into K-rich pegmatite (pink) and albite-rich pegmatite (white).

### 1. K-rich pegmatite

K-rich pegmatite is coarse to very coarse-grained rock with a pink color. It comprised mainly of K-feldspars and quartz with few amounts of albite, muscovite, and mafic minerals. Accessory minerals include Fe-Ti oxides, Nb-Ta oxides, spodumene, beryl, monazite, apatite, zircon, fergusonite, xenotime, fluorite, pyrochlore, bastnaesite and samaerskite.

K-feldspar is the essential mineral and occurs as coarse-grained, subhedral to anhedral crystals of orthoclase and microcline. Orthoclase is intergrown with albite forming perthitic texture, while microcline shows tartan twinning (Fig. 5A). Some large crystals of K-feldspars enclose small crystals of albite (Fig. 5B) and/or iron oxides and zircon. Quartz occurs as anhedral large crystals showing undulose extinction and as inclusions in K-feldspars and muscovite. Few albite crystals are corroded by the latter muscovite, suggesting the muscovitization is slightly later than the albitization. Muscovite occurs as large crystals with subhedral to anhedral outlines. It is characterized by one set of cleavage and high interference color (Fig. 5C). Few anhedral amphibole crystals are observed in the K-rich pegmatite.

Spodumene is mostly subhedral but locally euhedral. It encloses minute crystals of cassiterite, Nb-Ta oxides, and apatite. Albitization and muscovitization of spodumene commonly occur along cleavages, fractures, and crystal borders of the host primary phases. Rarely, the rims of spodumene crystals are partially replaced by a fine-grained, fibrous intergrowth of quartz, muscovite, and apatite-producing myrmekitic boundaries. Few late zinnwaldite crystals are formed along the rims of primary spodumene and muscovite, suggesting the ultimate elevation of Li contents in the melt/fluid. Some spodumene crystals are surrounded by an albite rim and then by muscovite. This indicates that the muscovitization was established after the previous albitization of spodumene, rather than the direct conversion of spodumene to muscovite.

Opaque minerals include Nb-Ta and Fe-Ti oxides. Nb-Ta oxides occur as fine-grained elongate-prismatic, blocky, or platy crystals, euhedral to subhedral in shape and disseminated to intergrown with spodumene, primary muscovite, and albite or among the grains of silicate minerals. Minute crystals of zircon occur fillings of cavities and fractures in Nb-Ta oxides. Zoning patterns in Nb-Ta oxides observed using BSE imaging including: (1) normal zonation, which shows Ta-rich rims and Nb-rich cores, (2) oscillatory zonation, which is characterized by regular, alternating changes of Nb- and Ta-rich zones, and (3) patchy zonation, which usually occurs anhedral to euhedral grains, and overprints earlier normal zoning.

### 2. Albite rich pegmatite

Albite rich pegmatite is less common than K-rich pegmatite. It is medium-grained with white colour. It consists essentially of albite, quartz, K-feldspar, biotite and muscovite. The accessory minerals include opaques, fluorite, and zircon. Albite is the most common mineral and occurs as euhedral to anhedral prismatic crystals characterized by lamellar twinning. Some albite crystals show bent and broken twin planes due to later deformation (Fig. 5D). Some albite crystals are highly altered to sericite and muscovite and others are kaolinitized in the core of the crystal. K-feldspar crystals show perthitic texture and cross-hatching of microcline. Few crystals of the K-feldspars include small inclusions of quartz and muscovite. Few quartz crystals are graphically intergrown with albite forming graphic texture. Chlorite fibers and aggregates are found as the alteration product in biotite. Muscovite is found as small flakes among the other constituents.

## Analytical methods

### 1. Whole-rock chemical analyses

Based on the petrographic studies, minimally weathered samples of Ras Al Baroud pegmatite were selected for whole-rock analyses at the GeoAnalytical Lab, Washington State University (WSU), USA. The rock samples were crushed using an agate grinding bowl. The crushed samples were further ground using an agate mortar. The concentrations of major and some trace elements were determined via X-ray fluorescence (Thermo ARL XRF Spectrometer). Each powdered sample was weighed, mixed with two parts di-lithium tetraborate flux, fused at 1000 °C in a muffle furnace, and cooled. The loss on ignition (LOI) was determined by the weight difference after ignition at

1000 °C. The resulting bead was reground, re-fused, and polished on diamond lap to produce a smooth, flat surface for analysis. The calibration standard was reference material 650 CC from USGS standard rock powder GSP2. The detection limits for the major oxides and trace elements are available online from

the Geo Analytical Lab (<https://environment.wsu.edu/facilities/geoanalytical-lab>). The precision of the XRF analyses calculated from duplicate samples was better than 1% for most major elements and better than 4% for most trace elements (except V, Cr, Ni and Sc).

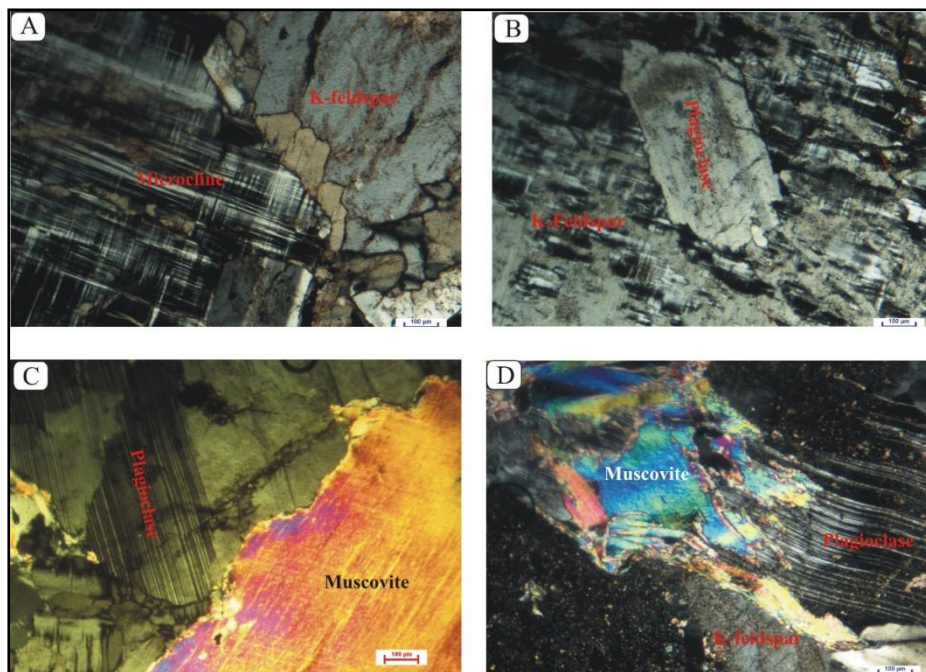


**Fig. 5.** (A) Microcline showing tartan twinning, (B) Albite enclosed in K-feldspar, (C) Anhedral muscovite crystal, and (D) Bent twin planes in albite.

## 2. Electron microprobe analysis (EMPA)

Major element compositions of feldspars muscovite and Nb-Ta oxides were determined by JEOL JXA-8530F field-emission electron microprobe (EMPA) at the University of Western Ontario (Canada). Operating conditions were an accelerating voltage of 20 kV probe current, beam current of 40-60 nA accelerating voltage, and spot sizes between 1 and 2 µm. Many of natural and synthetic mineral standards are used and a ZAF matrix correction is applied. Standards used for data correction were synthetic orthoclase for K, albite for Na, rutile for Ti, chromediopside for Si and Ca, olivine for Mg, magnetite for Fe, rhodonite for Mn, and pure metals for Nb, Ta. Analytical uncertainties are better than 5%.

### Mineral chemistry

The analyzed minerals include feldspars, muscovite, and Nb-Ta oxides. Chemical composition, structural formulae, based on 8 oxygens, and end-member components of all analyzed feldspars are given in **Tables 1 & 2**. According to the nomenclature given by **Deer et al., [17]**, the analyzed feldspar crystals are classified as K-feldspar and albite (**Fig. 6**). All the

analyzed K-feldspar crystals are homogenous with orthoclase composition (91 to 96 Or %). Albite has high Na<sub>2</sub>O content (11.08 to 11.29 wt. %) The analyzed albite crystals are pure with high albite contents (96.98 Ab %) and very low An content (2-4 %).

Compositions of muscovite with calculated structural formulae, based on 22 oxygens, are given in **Tables 3 & 4**. The chemical analysis of muscovites classifies them as primary and secondary muscovites using the discrimination Ti-Mg-Na ternary diagram after **Miller et al., [18]** (**Fig. 7**). The primary muscovite contains 0.45 to 0.62 TiO<sub>2</sub>, 30.76 to 31.73 wt. % Al<sub>2</sub>O<sub>3</sub>, 5.30 to 4.06 wt. % FeO, 0.30 to 0.54 wt. % MnO<sub>2</sub>, and 0.36 to 0.43 wt. Na<sub>2</sub>O. In comparison with primary muscovite, the secondary muscovite is enriched in FeO (6.54-7.27 wt. %) and depleted in TiO<sub>2</sub> (0.06-0.19 wt. %), Al<sub>2</sub>O<sub>3</sub> (27.59-29.82 wt. %) and Na<sub>2</sub>O (0.06-0.15 wt. %). The primary muscovite has TiO<sub>2</sub> > 0.4 wt. % comparable to muscovite of magmatic origin [19-20].

The Nb-Ta oxides are analyzed in the K-rich pegmatite and include columbite and tantalite. Chemical compositions and structural formulae of

Nb-Ta oxides are given in **Tables 5 & 6**. On the “columbite quadrilateral” diagram, the analyzed Nb-Ta oxides are plotted on the Mn-dominant side of columbite and tantalite (**Fig. 8**). Columbite displays very wide range of Nb<sub>2</sub>O (42.2-62.61 wt.%), Ta<sub>2</sub>O<sub>5</sub>(15.66-35.41wt.%), FeO (5.97-8.28 wt.%), and MnO (10.56-13.15 wt.%). This wide range in

composition can be attributed to the presence of zoning. Columbite has Mn/(Mn+Fe) ratios from 0.59 to 0.69 and Ta/(Nb+Ta) ratios from 0.13 to 0.33. Tantalite-(Mn) is recorded as rims around the columbite. Tantalite has Ta/(Nb+Ta) ratios from 0.52 to 0.64 and Mn/(Mn+Fe) ratios from 0.58-0.61.

**Table 1.** Electron microprobe analyses of K-feldspars in pegmatite of Ras Al-Baroud.

Spot No.	1	2	3	4	5	6	7	8	9	10
SiO <sub>2</sub>	64.89	64.98	65.08	64.99	64.9	64.84	64.8	65.02	64.92	64.82
TiO <sub>2</sub>	0.01	<d.l.	0.01	<d.l.	0.01	0.02	0.01	0.01	0.01	0.01
Al <sub>2</sub> O <sub>3</sub>	18.25	18.21	18.4	18.45	18.19	18.35	18.32	18.37	18.26	18.27
FeO*	0.24	0.12	0.22	0.27	0.11	0.35	0.18	0.28	0.26	0.17
MnO	0.01	0.01	0.01	<d.l.	0.02	0.02	0.02	<d.l.	0.01	0.01
MgO	<d.l.	0.01	0.01	0.01	0.01	0.01	0.01	0.01	0.01	0.01
CaO	0.03	0.04	0.07	0.03	0.03	0.07	0.04	0.06	0.06	0.06
Na <sub>2</sub> O	0.56	0.57	0.91	0.41	0.45	0.65	0.59	0.69	0.72	0.55
K <sub>2</sub> O	15.77	15.78	15.3	15.99	15.9	15.6	15.73	15.65	15.51	15.78
P <sub>2</sub> O <sub>5</sub>	0.01	<d.l.	<d.l.	<d.l.	0.02	0.01	0.01	<d.l.	0.02	0.01
Total	99.77	99.72	100.02	100.16	99.63	99.91	99.71	100.09	99.76	99.68
Structural formulae based on 8 oxygens										
Si	3.002	3.006	2.999	2.997	3.006	2.996	2.999	2.998	3.002	3.001
Ti	0.000	0.000	0.000	0.000	0.000	0.001	0.000	0.000	0.000	0.000
Al	0.995	0.993	0.999	1.003	0.993	0.999	0.999	0.998	0.995	0.997
Fe(ii)	0.009	0.005	0.008	0.010	0.004	0.014	0.007	0.011	0.010	0.007
Mn	0.000	0.000	0.000	0.000	0.001	0.001	0.001	0.000	0.000	0.000
Mg	0.000	0.001	0.001	0.001	0.001	0.001	0.001	0.001	0.001	0.001
Ca	0.001	0.002	0.003	0.001	0.001	0.003	0.002	0.003	0.003	0.003
Na	0.050	0.051	0.081	0.037	0.040	0.058	0.053	0.062	0.065	0.049
K	0.931	0.931	0.899	0.941	0.939	0.919	0.929	0.920	0.915	0.932
End-members										
Or	94.73	94.60	91.39	96.10	95.73	93.71	94.41	93.44	93.13	94.68
Ab	5.11	5.19	8.26	3.75	4.12	5.94	5.38	6.26	6.57	5.02
An	0.15	0.20	0.35	0.15	0.15	0.35	0.20	0.30	0.30	0.30

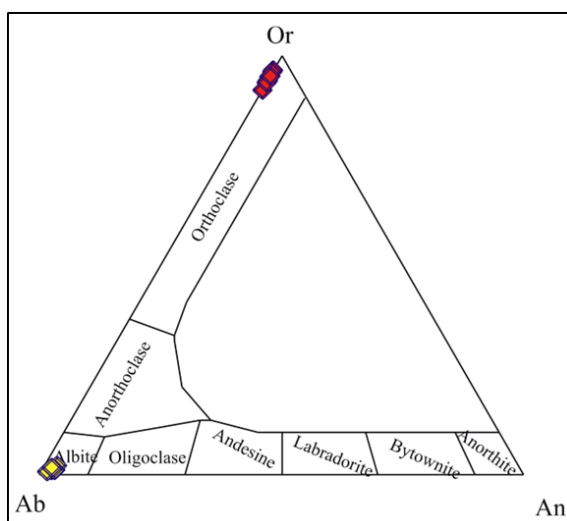


**Fig. 6.** Or-Ab-An ternary diagram of the classification of feldspars [17].

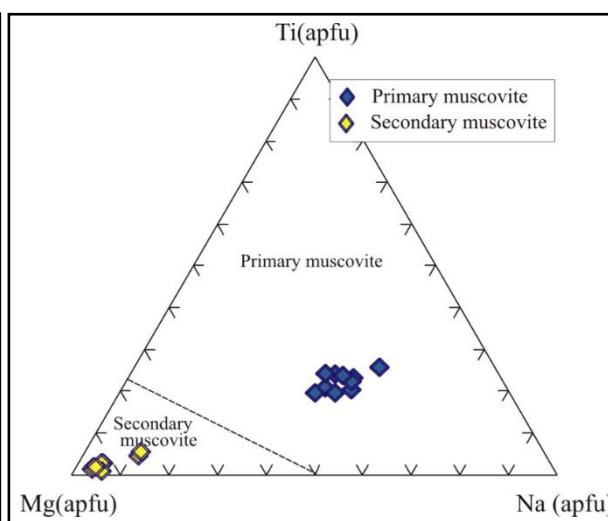


**Fig. 7.** Mg-Ti-Na ternary diagram for the compositional fields of muscovite after [18].

**Table 2.** Electron microprobe analyses of albite in pegmatite of Ras Al-Baroud.

Spot No.	1	2	3	4	5	6	7	8	9	10
SiO <sub>2</sub>	68.13	68.25	67.89	68.43	67.52	67.88	67.63	67.76	67.52	68.35
TiO <sub>2</sub>	0.01	0.01	0.02	<d.l.	<d.l.	0.01	0.01	0.01	0.01	0.02
Al <sub>2</sub> O <sub>3</sub>	20.07	19.01	18.98	19	20.04	20.21	19.97	19.92	20.04	19.91
FeO*	0.19	0.39	0.44	0.1	0.68	0.49	0.44	0.22	0.49	0.37
MnO	0.02	0.01	0.01	0.02	0.01	<d.l.	0.01	0.03	0.01	0.02
MgO	0.01	0.01	0.01	0.01	0.03	0.03	0.03	0.01	0.02	0.02
CaO	0.34	0.28	0.36	0.17	0.46	0.49	0.47	0.35	0.46	0.29
Na <sub>2</sub> O	11.08	11.15	11.11	11.19	11.11	11.09	11.29	11.1	11.19	11.2
K <sub>2</sub> O	0.18	0.19	0.27	0.13	0.39	0.2	0.18	0.25	0.2	0.3
P <sub>2</sub> O <sub>5</sub>	<d.l.	0.01	<d.l.	<d.l.	<d.l.	<d.l.	0.01	0.01	<d.l.	<d.l.
Total	100.01	99.29	99.09	99.04	100.24	100.41	100.03	99.65	99.95	100.47
Structural formulae based on 8 oxygens										
Si	2.976	3.005	2.999	3.013	2.958	2.962	2.964	2.974	2.961	2.978
Ti	0.000	0.000	0.001	0.000	0.000	0.000	0.000	0.000	0.000	0.001
Al	1.033	0.986	0.988	0.986	1.035	1.039	1.031	1.030	1.036	1.022
Fe(ii)	0.007	0.014	0.016	0.004	0.025	0.018	0.016	0.008	0.018	0.013
Mn	0.001	0.000	0.000	0.001	0.000	0.000	0.000	0.001	0.000	0.001
Mg	0.001	0.001	0.001	0.001	0.002	0.002	0.002	0.001	0.001	0.001
Ca	0.016	0.013	0.017	0.008	0.022	0.023	0.022	0.016	0.022	0.014
Na	0.938	0.952	0.952	0.955	0.944	0.938	0.959	0.945	0.952	0.946
K	0.010	0.011	0.015	0.007	0.022	0.011	0.010	0.014	0.011	0.017
End-members										
Or	1.04	1.09	1.55	0.75	2.21	1.14	1.01	1.44	1.14	1.71
Ab	97.31	97.55	96.72	98.42	95.60	96.50	96.76	96.88	96.67	96.91
An	1.65	1.35	1.73	0.83	2.19	2.36	2.23	1.69	2.20	1.39

**Table 3.** Electron microprobe analyses of primary muscovite in in Ras Al-Baroud pegmatite

Spot No.	1	2	3	4	5	6	7	8	9	10
SiO <sub>2</sub>	45.16	45.69	45.64	45.41	45.55	45.6	46.19	45.45	45.92	45.94
TiO <sub>2</sub>	0.46	0.54	0.59	0.51	0.49	0.51	0.56	0.45	0.62	0.5
Al <sub>2</sub> O <sub>3</sub>	31.73	31.37	30.93	30.83	30.9	31.19	30.76	30.97	31.59	31.08
FeO*	4.06	4.54	5.3	5.12	4.8	4.48	5.02	5.04	4.22	4.81
MnO	0.46	0.45	0.55	0.47	0.34	0.54	0.33	0.42	0.33	0.3
MgO	0.37	0.25	0.41	0.34	0.34	0.35	0.51	0.41	0.46	0.51
CaO	0.13	0.1	0.13	0.12	0.13	0.11	0.17	0.13	0.11	0.12
Na <sub>2</sub> O	0.41	0.41	0.4	0.39	0.39	0.36	0.43	0.39	0.39	0.4
K <sub>2</sub> O	9.8	9.86	9.92	9.71	9.85	9.87	10.02	9.73	9.97	9.95
Total	92.58	93.2	93.86	92.9	92.77	92.99	93.99	92.97	93.6	93.6
Structural formulae based on 24 oxygens										
Si	6.279	6.322	6.306	6.324	6.340	6.326	6.358	6.320	6.316	6.338
Al iv	1.721	1.678	1.694	1.676	1.660	1.674	1.642	1.680	1.684	1.662
Al vi	3.478	3.439	3.344	3.383	3.409	3.426	3.348	3.395	3.436	3.391
Ti	0.048	0.056	0.061	0.054	0.051	0.053	0.058	0.047	0.064	0.052
Fe	0.472	0.525	0.613	0.597	0.559	0.519	0.577	0.586	0.485	0.554
Mn	0.055	0.052	0.064	0.055	0.040	0.063	0.038	0.050	0.038	0.034
Mg	0.076	0.052	0.085	0.070	0.071	0.071	0.104	0.085	0.093	0.105
Ca	0.019	0.014	0.019	0.018	0.019	0.016	0.025	0.019	0.017	0.018
Na	0.111	0.109	0.106	0.106	0.105	0.097	0.115	0.104	0.105	0.106
K	1.737	1.741	1.749	1.725	1.749	1.746	1.759	1.725	1.748	1.751

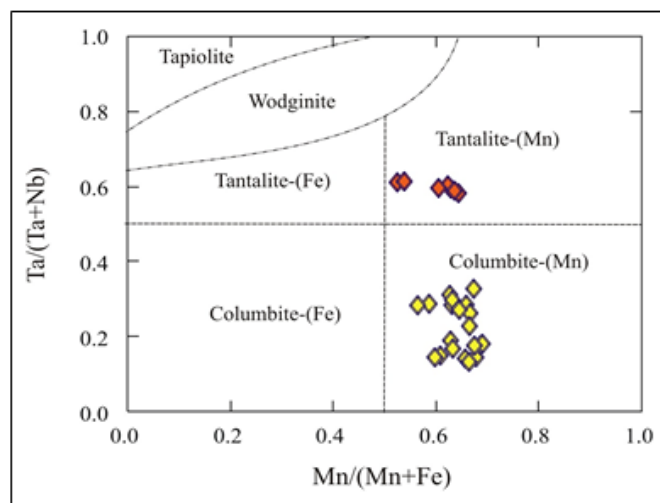


**Fig. 8.** Chemical composition and nomenclature of the Ta-Nb oxides based on Ta/(Ta+Nb) vs. Mn/(Mn+Fe) ratios.

**Table 4.** Electron microprobe analyses of secondary muscovite in Ras Al-Baroud pegmatite

Spot No	1	2	3	4	5	6	7	8	9
SiO <sub>2</sub>	44.74	44.8	45.05	45.27	44.66	44.97	45.14	44.68	44.97
TiO <sub>2</sub>	0.09	0.1	0.14	0.15	0.08	0.14	0.19	0.06	0.09
Al <sub>2</sub> O <sub>3</sub>	28.73	27.82	28.62	29.04	27.59	29.15	29.82	27.77	27.87
FeO*	7	6.96	6.54	6.85	7.06	6.27	6.23	7.27	7.23
MnO	0.53	0.54	0.37	0.32	0.58	0.33	0.18	0.68	0.49
MgO	2.1	2.11	2.07	1.34	2.17	2.06	1.39	2.24	1.98
CaO	0.14	0.14	0.17	0.24	0.13	0.16	0.23	0.11	0.19
Na <sub>2</sub> O	0.08	0.06	0.09	0.14	0.06	0.08	0.15	0.1	0.06
K <sub>2</sub> O	9.76	9.62	9.87	10.36	9.59	9.89	10.06	9.65	9.76
Total	93.16	92.14	92.91	93.72	91.92	93.04	93.39	92.57	92.65
Structural formulae based on 24 oxygens									
Si	6.297	6.371	6.340	6.338	6.374	6.308	6.304	6.345	6.372
Al <sup>iv</sup>	1.703	1.629	1.660	1.662	1.626	1.692	1.696	1.655	1.628
Al <sup>vi</sup>	3.065	3.035	3.086	3.132	3.015	3.127	3.213	2.994	3.028
Ti	0.010	0.010	0.014	0.016	0.008	0.015	0.020	0.006	0.010
Fe	0.824	0.828	0.769	0.802	0.843	0.736	0.727	0.863	0.856
Mn	0.063	0.065	0.044	0.038	0.070	0.039	0.021	0.081	0.059
Mg	0.441	0.447	0.435	0.280	0.461	0.431	0.289	0.475	0.418
Ca	0.021	0.021	0.026	0.037	0.019	0.024	0.034	0.016	0.028
Na	0.022	0.017	0.024	0.038	0.017	0.022	0.040	0.028	0.017
K	1.752	1.746	1.771	1.850	1.746	1.769	1.792	1.749	1.765

## Geochemistry

Within the studied area, granitic pegmatite dikes have a close spatial correlation and geochemical affinity with the granitic rocks of Ras Al-Baroud intrusion [13]. Whole-rock geochemical data (major, trace and rare-earth elements) of Ras Al-Baroud pegmatite are given in Table 7. The pegmatite extends over a range in SiO<sub>2</sub> from 75.43 to 82.72 wt.%. Trace element concentrations vary widely among pegmatites. Some samples have marked enrichment in some elements and others are depleted.

Geochemically, the Ras Al-Baroud pegmatite shows distinctively low contents of CaO, MgO, and Sr in

contrast to elevated concentrations of alkalis, Rb, Nb, Y, Ta, Hf, Zr, and rare-earth elements (REE); these are common characteristics of post-collisional rare-metal-bearing A-type rocks.

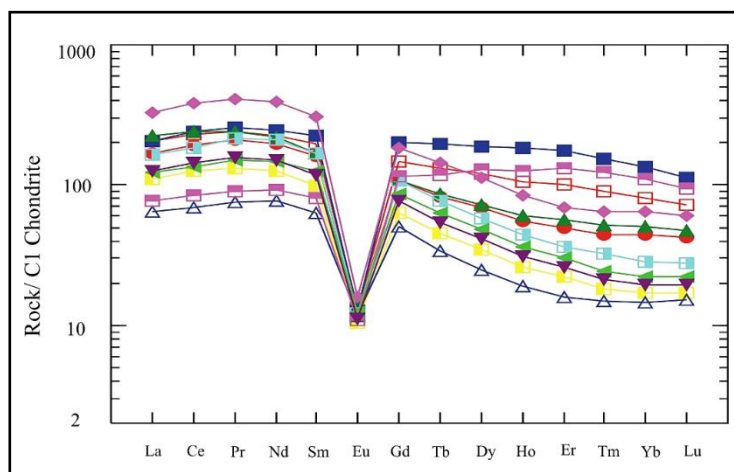
The analyzed pegmatite samples have a wide range of total REE contents (136-683 ppm). This wide range in REE can be attributed to the wide variations in the accessory minerals in the pegmatite. The chondrite-normalized REE patterns are presented in Figure (9). The analyzed samples display essentially subparallel REE patterns. All samples have pronounced negative Eu anomalies (Eu/Eu\* = 0.07-0.21).

**Table 5.** Electron microprobe analyses of columbite in pegmatites of Ras Al-Baroud

Spot No.	1	2	3	4	5	6	7	8	9	10
SiO2	0.67	1.82	1	0.96	0.27	0.37	1.14	0.71	0.42	0.9
TiO2	0.08	0.11	0.1	0.12	0.06	0.08	0.13	0.1	0.07	0.16
Al2O3	<d.l.	0.02	<d.l.	<d.l.	<d.l.	<d.l.	0.01	<d.l.	<d.l.	<d.l.
FeO*	6.91	7.82	7.32	5.97	6.35	6.08	8.28	7.08	6.02	6.42
MnO	12.99	10.91	12.16	12.08	13.11	13.09	10.56	11.98	13.15	12.19
MgO	<d.l.	<d.l.	<d.l.	<d.l.	<d.l.	0.01	<d.l.	<d.l.	0.01	<d.l.
CaO	0.02	0.01	0.07	0.12	0.01	0.01	<d.l.	0.02	0.02	0.05
Na2O	0.01	0.03	0.04	0.07	<d.l.	0.01	0.02	<d.l.	<d.l.	0.03
K2O	0.01	<d.l.	<d.l.	<d.l.	<d.l.	<d.l.	<d.l.	0.01	0.01	<d.l.
P2O5	0.01	0.01	0.01	0.01	0.01	0.02	<d.l.	0.01	0.01	0.01
Nb2O5	61.45	47.09	56.6	44.2	61.85	58.39	48.07	59.41	58	47.67
Ta2O5	16.5	31.29	21.68	35.41	17.06	20.59	31.29	19.6	21	31.21
SnO2	0.12	0.08	0.08	0.09	0.14	0.12	0.07	0.13	0.13	0.08
Total	98.75	99.2	99.04	99.02	98.86	98.74	99.56	99.02	98.81	98.72
Structural formula on the basis of 6 oxygen atoms										
Si	0.01	0.03	0.02	0.02	0.00	0.01	0.02	0.01	0.01	0.01
Al	0.00	0.00	0.00	0.00	0.00	0.00	0.00	0.00	0.00	0.00
Ti	0.00	0.00	0.00	0.00	0.00	0.00	0.00	0.00	0.00	0.00
Fe	0.10	0.11	0.10	0.08	0.09	0.08	0.12	0.10	0.08	0.09
Mn	0.18	0.15	0.17	0.17	0.18	0.18	0.15	0.17	0.19	0.17
Mg	0.00	0.00	0.00	0.00	0.00	0.00	0.00	0.00	0.00	0.00
Ca	0.00	0.00	0.00	0.00	0.00	0.00	0.00	0.00	0.00	0.00
Na	0.00	0.00	0.00	0.00	0.00	0.00	0.00	0.00	0.00	0.00
Nb	0.46	0.35	0.43	0.33	0.47	0.44	0.36	0.45	0.44	0.36
Ta	0.07	0.14	0.10	0.16	0.08	0.09	0.14	0.09	0.10	0.14
Mn/(Mn+Fe)	0.66	0.59	0.63	0.67	0.68	0.69	0.56	0.63	0.69	0.66
Ta/(Ta+Nb)	0.14	0.29	0.19	0.33	0.14	0.18	0.28	0.17	0.18	0.28
Spot No.	1	2	3	4	5	6	7	8	9	10
SiO2	2	0.93	1.25	0.68	0.92	0.23	1.74	0.56	0.76	0.75
TiO2	0.21	0.07	0.16	0.09	0.1	0.09	0.14	0.13	0.11	0.12
Al2O3	<d.l.	0.03	<d.l.	<d.l.	<d.l.	0.01	<d.l.	0.02	<d.l.	<d.l.
FeO*	6.96	7.7	6.99	6.29	6.23	6.69	6.8	8.01	6.77	6.36
MnO	11.51	11.77	11.73	12.81	12.21	12.99	11.47	11.71	12.09	12.41
MgO	<d.l.									
CaO	0.05	0.01	0.01	0.06	0.03	0.01	0.02	0.01	0.01	0.01
Na2O	0.02	0.05	<d.l.	0.03	0.01	<d.l.	<d.l.	0.03	<d.l.	<d.l.
K2O	<d.l.	<d.l.	<d.l.	<d.l.	<d.l.	0.01	0.01	<d.l.	<d.l.	<d.l.
P2O5	<d.l.	0.01	<d.l.	0.01	0.01	0.01	0.01	<d.l.	0.01	<d.l.
Nb2O5	44.96	60.64	47.66	58.27	50	62.61	46.42	61.7	49.05	53.28
Ta2O5	33.54	17.39	31.07	20.43	29.31	15.66	32.4	17	30.04	25.84
SnO2	0.06	0.11	0.07	0.11	0.09	0.13	0.09	0.1	0.1	0.11
Total	99.33	98.69	98.96	98.75	98.91	98.41	99.09	99.25	98.93	98.86
Structural formula on the basis of 6 oxygen atoms										
Si	0.03	0.02	0.02	0.01	0.02	0.00	0.03	0.01	0.01	0.01
Al	0.00	0.00	0.00	0.00	0.00	0.00	0.00	0.00	0.00	0.00
Ti	0.00	0.00	0.00	0.00	0.00	0.00	0.00	0.00	0.00	0.00
Fe	0.10	0.11	0.10	0.09	0.09	0.09	0.09	0.11	0.09	0.09
Mn	0.16	0.17	0.17	0.18	0.17	0.18	0.16	0.17	0.17	0.17
Mg	0.00	0.00	0.00	0.00	0.00	0.00	0.00	0.00	0.00	0.00
Ca	0.00	0.00	0.00	0.00	0.00	0.00	0.00	0.00	0.00	0.00
Na	0.00	0.00	0.00	0.00	0.00	0.00	0.00	0.00	0.00	0.00
Nb	0.34	0.46	0.36	0.44	0.38	0.47	0.35	0.46	0.37	0.40
Ta	0.15	0.08	0.14	0.09	0.13	0.07	0.15	0.08	0.14	0.12
Mn/(Mn+Fe)	0.63	0.61	0.63	0.67	0.66	0.66	0.63	0.60	0.64	0.66
Ta/(Ta+Nb)	0.31	0.15	0.28	0.17	0.26	0.13	0.30	0.14	0.27	0.23

**Table 6.** Electron microprobe analyses of tantalite in pegmatites of Ras Al-Baroud

Spot No.	1	2	3	4	5	6	7
SiO <sub>2</sub>	2.05	2.07	3.87	1.96	2.06	3.35	2.53
TiO <sub>2</sub>	0.24	0.25	0.27	0.2	0.24	0.26	0.28
Al <sub>2</sub> O <sub>3</sub>	<d.l.	<d.l.	<d.l.	<d.l.	<d.l.	<d.l.	<d.l.
FeO*	6.35	5.89	8.09	6.47	6.12	7.9	6.73
MnO	10.58	10.45	8.79	10.51	10.51	9.06	10.13
MgO	<d.l.	<d.l.	<d.l.	<d.l.	<d.l.	<d.l.	<d.l.
CaO	0.16	0.04	0.01	0.01	0.1	0.01	0.02
Na <sub>2</sub> O	0.1	0.01	<d.l.	<d.l.	0.06	<d.l.	0.01
K <sub>2</sub> O	<d.l.	<d.l.	<d.l.	<d.l.	<d.l.	<d.l.	<d.l.
P <sub>2</sub> O <sub>5</sub>	0.01	<d.l.	<d.l.	<d.l.	<d.l.	<d.l.	<d.l.
Nb <sub>2</sub> O <sub>5</sub>	23.29	24.39	21.99	22.9	23.84	21.92	23.26
Ta <sub>2</sub> O <sub>5</sub>	56.34	56.12	57.03	57.38	56.23	57.38	56.54
SnO <sub>2</sub>	0.03	0.02	0.02	0.03	0.03	0.02	0.02
Total	99.14	99.22	100.06	99.44	99.18	99.88	99.51
Structural formula on the basis of 6 oxygen atoms							
Si	0.03	0.03	0.06	0.03	0.03	0.06	0.04
Al	0.00	0.00	0.00	0.00	0.00	0.00	0.00
Ti	0.00	0.00	0.00	0.00	0.00	0.00	0.00
Fe	0.09	0.08	0.11	0.09	0.09	0.11	0.09
Mn	0.15	0.15	0.12	0.15	0.15	0.13	0.14
Mg	0.00	0.00	0.00	0.00	0.00	0.00	0.00
Ca	0.00	0.00	0.00	0.00	0.00	0.00	0.00
Na	0.00	0.00	0.00	0.00	0.00	0.00	0.00
Nb	0.18	0.18	0.17	0.17	0.18	0.16	0.18
Ta	0.25	0.25	0.26	0.26	0.25	0.26	0.26
Mn/(Mn+Fe)	0.63	0.64	0.52	0.62	0.64	0.54	0.60
Ta/(Ta+Nb)	0.59	0.58	0.61	0.60	0.59	0.61	0.59

**Fig. 9.** Chondrite-normalized REE patterns for the pegmatite of Ras Al-Baroud.

## Petrogenesis

Pegmatite is a term used to describe an intrusive igneous rock with very large crystals that form in the later stages of a magma chamber's crystallization. Many previous studies focus on the sources of the pegmatite-forming magma. Some researchers proposed that the pegmatites originated from the granitic magma, by degree of fractional crystallization during ascent along faults [21-22].

Other researchers suggested that the pegmatite-forming magma was stemming largely from anatexis of metasedimentary rocks instead of fractionation products of granitic magma [23]. Still now, the role of magmatic and hydrothermal processes during the evolution of rare metals during the pegmatite-forming processes are still unclear.

In the Ras Al-Baroud area, the pegmatites appear to be the most fractionated member of the surrounding granites, most of which contain a common granitic

mineral assemblage along with rare metals bearing minerals (Nb–Ta oxides). Nb-Ta oxides in the studied pegmatite exhibit an evolution from Nb- to Ta-rich consisting of progressively fractional crystallization as observed in many other pegmatites worldwide [24 - 25]. The results show variable Mn# [Mn/(Mn+Fe)] values with the presence of a prominent trend of fractional crystallization. Mn# has been considered to be controlled in large part by the crystallization of tourmaline, garnet, apatite, and Nb-Ta oxides [2, 26]. However, tourmaline and garnet mineralization is rare in the Ras Al-Baroud pegmatites. Most of euhedral Nb-Ta oxides with simple zoning patterns indicate the crystallization is mainly a magmatic process. Oscillatory zoning is rare in our samples and probably reflects local fluctuations of melt composition during crystal growth. Irregular with patchy zoning patterns, indicates that early generations of Nb-Ta oxides subsequently underwent alteration. This is supported by the overprint of earlier formed homogenous columbite with normal zoning pattern by patchy zoning rich in tantalite.

In the Ras Al-Baroud pegmatite, the magmatic-hydrothermal transition is characterized by albitization and muscovitization of primary alkali feldspar, and resorption textures and patchy zoning of Nb-Ta oxides. Petrography showed that the muscovitization was established after the previous albitization. Greisenization is the result of interaction between the aqueous fluids and early-formed mineral phases including alkaline feldspar, and albite. The presence of Fe–Mn oxides in fractures and cleavage planes of primary minerals indicates that the hydrothermal fluids were enriched in Fe and Mn and/or contributed from country rock during the fluid migration.

Albitization in Ras Al-Baroud pegmatites is pervasive in some samples and shows a close relationship with mineralization of rare metals, especially in strongly mineralized pegmatites. From another perspective, the occurrence of widespread albitization indicates that H<sub>2</sub>O and volatile elements (F and P) are intensely enriched in the pegmatitic melt due to magmatic crystallization and fractionation before consolidation. The sudden change of the physio-chemical environment (e.g., depressurization, cooling, and fluid exsolution) leads to the supersaturation of rare elements in the melts. During this process, economically valuable Nb-Ta oxides mainly crystallize from the melts under disequilibrium conditions, as suggested by the patchy zoning of Nb-Ta oxides [27]. Therefore, albitization associated with pegmatites can be regarded as a favorable target for Ta–Nb exploration in Ras Al-Baroud area.

Although we do observe subsolidus re-equilibration textures and the formation of secondary minerals at the expense of primary minerals in the pegmatite, a magmatic origin for the hydrothermal solutions that affected these pegmatites is favored. This is supported by the presence of pegmatite at the outer margins of Ras Al-Baroud granites and by the gradational boundaries of these pegmatites. Extended fractional crystallization in Ras Al-Baroud granites eventually produced saturated, late-magmatic fluids. These fluids migrated towards the apex of the magma chamber, reacting with still hot but subsolidus granite and becoming increasingly focused into distinct channels and veins. This upward and outward mode of fluid migration led to pegmatites with gradational boundaries.

**Table 7.** Bulk chemical analyses of Ras Al-Baroud pegmatites, Eastern Desert, Egypt

Sample No.	RBP1	RBP2	RBP3	RBP4	RBP5	RBP6	RBP7	RBP8	RBP9	RBP10	RBP11
Major oxides (wt.%)											
SiO <sub>2</sub>	76.98	75.78	75.97	81.32	81.84	75.43	76.25	82.72	81.96	75.84	79.54
TiO <sub>2</sub>	0.16	0.24	0.2	0.09	0.03	0.12	0.29	0.12	0.08	0.2	0.09
Al <sub>2</sub> O <sub>3</sub>	11.99	8.96	10.09	9.69	9.72	11.78	8.35	8.18	9.2	10.07	8.75
Fe <sub>2</sub> O <sub>3</sub>	3.58	6.5	3.47	1.78	1.39	3.58	6.04	2.62	1.93	4.81	2.05
MnO	0.1	0.06	0.08	0.01	0.03	0.05	0.09	0.02	0.02	0.07	0.02
MgO	0.16	0.01	0.17	<dl	<dl	0.16	0.02	<dl	<dl	0.09	<dl
CaO	0.61	0.65	1.59	0.15	0.3	1.69	0.76	0.24	0.23	1.22	0.2
Na <sub>2</sub> O	1.55	2.53	2.08	2.47	3.34	2.16	2.76	1.97	2.59	2.96	3.24
K <sub>2</sub> O	3.66	3.7	3.54	4.4	3.09	3.87	2.78	3.77	3.75	2.83	4.44
P <sub>2</sub> O <sub>5</sub>	<dl	0.02	<dl	<dl	<dl	0.03	0.01	<dl	<dl	0.01	<dl
LOI	1.42	1.16	2.32	0.18	0.22	1.17	1.36	0.24	0.21	1.26	0.8
Total	100.21	99.61	99.51	100.09	99.96	100.04	98.71	99.88	99.97	99.36	99.13

**Table 7. Continue**

Sample No.	RBP1	RBP2	RBP3	RBP4	RBP5	RBP6	RBP7	RBP8	RBP9	RBP10	RBP11
<b>Trace elements (ppm)</b>											
Rb	234.7	38.7	162.1	76.1	63.8	150.7	57.8	63.1	67.7	104.2	66.9
Ba	69.2	65.7	656.4	290.4	42.7	685.4	39.5	274.7	202.6	362.4	248.2
Sr	33.8	40.2	39.1	47.4	21.0	58.0	22.1	46.1	38.2	40.1	42.6
Nb	179.3	319.2	127.4	48.2	28.8	342.9	97.1	30.4	52.5	220.0	99.7
Zr	295.8	544.3	489.9	404.0	464.6	298.9	554.7	509.1	459.3	426.8	443.8
Y	82.7	223.6	124.2	22.4	67.1	229.0	118.5	55.1	48.2	173.7	40.7
Zn	206.6	336.6	262.4	75.7	158.3	86.1	456.6	154.1	129.4	271.4	116.2
Cu	3.2	2.1	107.1	11.1	5.6	106.0	1.8	11.4	9.4	53.9	10.3
Ni	49.4	83.4	41.2	20.5	31.5	81.1	46.2	34.2	28.8	63.7	27.0
Co	67.6	62.7	24.6	165.7	81.6	58.5	62.8	152.4	133.2	60.6	145.9
Cr	35.1	30.3	8.9	69.9	37.4	22.4	34.9	63.3	56.9	28.6	61.5
V	16.5	5.9	22.3	10.1	3.2	14.0	2.1	10.1	10.1	14.0	9.7
Th	21.4	39.1	32.8	5.7	7.9	49.4	18.7	8.6	7.4	34.0	7.0
F	2560.2	879.2	2765.4	2881.6	1100.7	2738.0	978.2	2881.6	2881.6	2738.0	2795.1
Sc	1.3	2.5	3.0	0.5	1.0	1.4	3.1	1.0	0.8	2.3	0.8
Mo	0.4	0.2	0.1	0.4	0.1	0.2	0.4	0.8	0.4	0.3	0.5
Sn	8.8	10.7	10.7	5.1	4.8	4.6	12.9	4.4	4.0	8.7	2.9
Cs	2.1	<d.l.	<d.l.	<d.l.	2.1	1.8	<d.l.	<d.l.	1.1	<d.l.	<d.l.
Hf	14.1	21.8	20.7	13.9	15.5	14.7	21.4	17.6	15.7	18.0	15.3
Ta	13.7	5.0	10.6	0.2	0.4	12.5	3.3	0.5	0.4	7.9	0.3
W	6.6	4.0	1.9	9.6	4.5	3.9	3.9	8.9	7.7	3.9	8.4
Pb	2.5	5.2	18.0	6.6	2.7	20.4	3.2	6.2	5.2	11.8	5.8
U	2.5	18.2	5.8	2.6	2.2	20.7	2.6	3.1	2.6	11.7	2.7
<b>REE(ppm)</b>											
La	39.85	48.2	52.71	15.46	38.99	18.3	77.1	29.33	30.14	49.2	26.37
Ce	117.65	148.57	147.89	41.85	113.59	51.98	234.36	83.04	88.33	141.17	77.51
Pr	19.97	24.16	23.02	7.21	20.37	8.57	39.12	14.36	14.87	22.79	12.64
Nd	92.57	114.09	102.97	36.36	97.17	42.66	181.9	69.26	69.93	105.28	59.03
Sm	24.64	34.49	25.58	9.66	25.63	12.33	47.16	19.31	18.15	29.75	15.19
Eu	0.76	0.74	0.68	0.69	0.7	0.63	0.93	0.73	0.64	0.78	0.6
Gd	22.02	41.67	22.19	10.41	22.24	23.84	37.46	17.92	15.7	30.15	13.12
Tb	3.08	7.28	3.23	1.28	2.89	4.39	5.4	2.37	2.04	4.9	1.7
Dy	17.48	47.38	18.47	6.32	14.84	32.99	28.79	12.28	10.44	30.89	8.71
Ho	3.12	10.36	3.43	1.08	2.48	7.21	4.82	2.03	1.75	6.02	1.46
Er	8.18	29.08	9.41	2.66	6.03	22	11.53	5.03	4.34	16.76	3.66
Tm	1.14	3.91	1.31	0.38	0.83	3.13	1.63	0.62	0.54	2.28	0.46
Yb	7.47	22.69	8.59	2.46	4.85	18.81	10.88	3.81	3.27	13.85	2.86
Lu	1.08	2.89	1.2	0.39	0.71	2.37	1.54	0.56	0.49	1.83	0.43
Eu/Eu*	0.10	0.06	0.09	0.21	0.09	0.11	0.07	0.12	0.12	0.08	0.13
(La/Yb) <sub>n</sub>	3.61	1.44	4.15	4.25	5.44	0.66	4.79	5.21	6.23	2.40	6.24
(La/Sm) <sub>n</sub>	1.02	0.88	1.30	1.01	0.96	0.94	1.03	0.96	1.05	1.04	1.10
(Gd/Lu) <sub>n</sub>	2.50	1.77	2.27	3.27	3.84	1.23	2.98	3.92	3.93	2.02	3.74
(La/Lu) <sub>n</sub>	3.78	1.71	4.50	4.06	5.63	0.79	5.13	5.37	6.30	2.75	6.28
Eu/Eu*	0.10	0.06	0.09	0.21	0.09	0.11	0.07	0.12	0.12	0.08	0.13

## Summary

- The Neoproterozoic rock units cropping in the Ras Al-Baroud area represent a part of the Arabian-Nubian Shield. They include syntectonic and post-collisional granites that are associated with rare-metal bearing pegmatites. Pegmatites of Ras Al-Baroud are coarse-grained and variable in their shapes and sizes. They occur as dikes and lenticular bodies inside the pluton and along the marginal parts.

- In few outcrops, the Ras Al-Baroud pegmatites are commonly affected by intense metasomatic-hydrothermal alteration resulting in albitization and greisenization, especially close to contact with the host rocks.

- The granitic pegmatites in the study area are coarse-grained and show a sequence of zones including

microcline pegmatite, microcline albite pegmatite, and albite pegmatite. Mineralization of Ras Al-Baroud intrusion is mainly concentrated in the pegmatite outcrops and, to a lesser extent, in Ras Al-Baroud granite. Based on colour and mineralogical composition, the Ras Al-Baroud pegmatites are distinguished into K-rich pegmatite (pink) and albite-rich pegmatite (white).

- Textural features of Nb-Ta minerals indicate a magmatic origin of majority of crystals with influence of a late- to post-magmatic replacement. The accumulation of volatiles and trace elements ultimately led to the development of pegmatites and veins at the end of the magmatic phase.

## References

- [1] Černý, P., London, D., Novák, M., Granitic Pegmatites as Reflections of Their Sources. *Elements*, (2012), 8, 289–294. [DOI: 10.2113/gselements.8.4.289](https://doi.org/10.2113/gselements.8.4.289)
- [2] London, D., Ore-forming processes within granitic pegmatites. *Ore Geology Reviews*, (2018), 101, 349–383. <https://doi.org/10.1016/j.oregeorev.2018.04.020>
- [3] Kaeter, D., Barros, R., Menuge, J.F., Chew, D.M., The magmatic–hydrothermal transition in rare-element pegmatites from southeast Ireland: LA-ICP-MS chemical mapping of muscovite and columbite–tantallite. *Geochimica et Cosmochimica Acta*, (2018), 240, 98–130. [DOI: 10.1016/j.gca.2018.08.024](https://doi.org/10.1016/j.gca.2018.08.024)
- [4] Michaud, J.A.S., Pichavant, M., Magmatic fractionation and the magmatic hydrothermal transition in rare metal granites: evidence from argemela (central Portugal). *Geochimica et Cosmochimica Acta*, (2020), 289, 130–157. [DOI:10.1016/j.gca.2020.08.022](https://doi.org/10.1016/j.gca.2020.08.022)
- [5] Azer, M.K., Asimow, P.D., Petrogenetic Evolution of the Neoproterozoic Igneous Rocks of Egypt. In *The Geology of the Egyptian Nubian Shield*, (2021), pp. 343-382, Springer, Cham. [DOI: 10.1007/978-3-030-49771-2\\_13](https://doi.org/10.1007/978-3-030-49771-2_13)
- [6] Stern, R.J., Arc assembly and continental collision in the Neoproterozoic East African Orogen: implications for the consolidation of Gondwanaland. *Annual review of earth and planetary sciences*, (1994), 22(1), 319-351. <https://doi.org/10.1146/annurev.earth.22.050194.001535>
- [7] Azer, M.K., Tectonic significance of Late Precambrian calc-alkaline and alkaline magmatism in Saint Katherine area, South Sinai, Egypt. *Geologica Acta*, (2021), 5 (3), 255–272.
- [8] Jarrar, G.H., Manton, W.I., Stern, R.J., Zachmann, F., Late Neoproterozoic A-type granites in the northernmost Arabian-Nubian Shield formed by fractionation of basaltic melts. *Chem Erde*, (2008), 68, 295–312. [DOI: 10.1016/j.chemer.2006.09.002](https://doi.org/10.1016/j.chemer.2006.09.002)
- [9] Farahat, E.S., Azer, M.K., Post-collisional magmatism in the northern Arabian-Nubian Shield: the geotectonic evolution of the alkaline suite at Gebel Tarbush area, south Sinai, Egypt. *Chem Erde*, (2011), 71, 247–266. [DOI: 10.1016/j.chemer.2011.06.003](https://doi.org/10.1016/j.chemer.2011.06.003)
- [10] Lundmark, A.M., Andresen, A., Hassan, M.A., Augland, L.E., Boghdady, G.Y., Repeated magmatic pulses in the East African Orogen in the Eastern Desert, Egypt: An old idea supported by new evidence. *Gondwana Research*, (2012), 22(1), 227–37. [DOI: 10.1016/j.gr.2011.08.017](https://doi.org/10.1016/j.gr.2011.08.017)
- [11] Khalil, A.E.S., Obeid M.A., Azer, M.K., Asimow, P.D., Geochemistry and petrogenesis of post-collisional alkaline and peralkaline granites of the Arabian-Nubian Shield: a case study from the southern tip of Sinai Peninsula, Egypt. *International Geological Review*, (2018), 60(8), 998–1018. <https://doi.org/10.1080/00206814.2017.1364672>
- [12] Abuamarah, B.A., Azer, M.K., Seddik, A.M., Asimow, P.D., Guzman, P., Fultz, B.T., Wilner, M.J., Dalleska, N., Darwish, M.H., Magmatic and post-magmatic evolution of post-collisional rare-metal bearing granite: The Neoproterozoic Homrit Akarem Granitic Intrusion, south Eastern Desert of Egypt, Arabian-Nubian Shield. *Geochemistry* 82, (2022), p.125840. <https://doi.org/10.1016/j.chemer.2021.125840>
- [13] Abuamarah, B.A., Alzahrán, H., Matta, M.J., Azer, M.K., Asimow, P.D., Darwish, M.H., Petrological, geochemical and geodynamic evolution of the Wadi Al-Baroud granitoids, north Arabian-Nubian shield, Egypt. *Journal of African Earth Sciences*, (2023), p.105044. [DOI:10.1016/j.jafrearsci.2023.105044](https://doi.org/10.1016/j.jafrearsci.2023.105044)
- [14] Abd El-Wahed, M., Hamimi, Z., The Egyptian Nubian Shield within the Frame of the Arabian–Nubian Shield. *The Geology of the Egyptian Nubian*

- Shield, (2021), pp.15-51. [DOI:10.1007/978-3-030-49771-2\\_2](https://doi.org/10.1007/978-3-030-49771-2_2)
- [15] Heikal, M.T.S., Khedr, M.Z., Abd El Monsef, M., Gomaa, S.R., Petrogenesis and geodynamic evolution of neoproterozoic Abu Dabbab albite granite, central Eastern Desert of Egypt: petrological and geochemical constraints. *Journal of African Earth Sciences*, (2019), 158, p.103518. [DOI: 10.1016/j.jafrearsci.2019.103518](https://doi.org/10.1016/j.jafrearsci.2019.103518)
- [16] Moussa, H.E., Asimow, P.D., Azer, M.K., Abou El Maaty, M.A., Akarish, A.I., Yanni, N.N., Mubarak, H.S., Wilner, M.J., El sagheer, M.A., Magmatic and hydrothermal evolution of highly-fractionated rare-metal granites at Gabal Nuweibi, Eastern Desert, Egypt. *Lithos*, (2021), 400, p.106405.
- [17] Deer, W.A., Howie, R.A., Zussman, J., An introduction to the rock forming minerals. Second Edition, Longman Scientific and Technical, London, (1992), 696pp. <https://doi.org/10.1180/minmag.1992.056.385.20>
- [18] Miller, C.F., Stoddard, E.F., Bradfish, L.J., Dollase, W.A., Composition of plutonic muscovite: genetic implications. *Canadian Mineralogist*, (1981), 19(1), 25-34.
- [19] Anderson, J.L., Rowley, M.C., Synkinematic intrusion of peraluminous and associated metaluminous granitic magmas, Whipple Mountains, California. *The Canadian Mineralogist* (1981), 19(1), 83-101. <https://api.semanticscholar.org/CorpusID:53709151>
- [20] Zen, E.A., Phase relations of peraluminous granitic rocks and their petrogenetic implications. *Annual Review of Earth and Planetary Sciences*, (1988), 16(1), 21-51. <https://doi.org/10.1146/annurev.ea.16.050188.00032>
- [21] Li, J.K., Wang, D.H., Fu, X.F.,  $^{40}\text{Ar}/^{39}\text{Ar}$  ages of the Ke'eryin pegmatite type rare metal deposit, western Sichuan, and its tectonic significances. *Acta Geologica Sinica*, (2006), 80, 843–848 (In Chinese with English abstract).
- [22] Ma, S.C., Wang, D.H., Liu, S.B., Sun, Y., Guo, W.M., Dai, H.Z., Liu, L.J., Li, C., Mineral chemistry of micas from Ke'eryin pegmatite type lithium orefield in western Sichuan and its indication for rare metal mineralization and prospecting. *Mineral Deposits*, (2019), 38 (4), 877–897 (in Chinese with English abstract).
- [23] Fei, G., Menuge, J.F., Li, Y., Yang, J., Deng, Y., Chen, C., Yang, Y., Yang, Z., Qin, L., Zheng, L., Petrogenesis of the Lijiagou spodumene pegmatites in Songpan-Garze Fold Belt, West Sichuan, China: Evidence from geochemistry, zircon, cassiterite and coltan U-Pb geochronology and Hf isotopic compositions. *Lithos*, (2020), 364, 105555. [DOI: 10.1016/j.lithos.2020.105555](https://doi.org/10.1016/j.lithos.2020.105555)
- [24] Badanina, E., Sitnikova, M., Gordienko, V., Melcher, F., Gäbler, H.E., Lodziak, J., Syritso, L., Mineral chemistry of columbite–tantalite from spodumene pegmatites of Kolmozero, Kola Peninsula (Russia). *Ore Geology Reviews*, (2015), 64, 720–735. <http://dx.doi.org/10.1016/j.oregeorev.2014.05.009>
- [25] Xing, C.M., Wang, C.Y., Wang, H., Magmatic-hydrothermal processes recorded by muscovite and columbite-group minerals from the Bailongshan rare-element pegmatites in the West Kunlun-Karakorum orogenic belt, NW China. *Lithos*, (2020), 364–365, 105507. [DOI: 10.1016/j.lithos.2020.105507](https://doi.org/10.1016/j.lithos.2020.105507)
- [26] Anderson, M.O., Lentz, D.R., McFarlane, C.R., Falck, H., A geological, geochemical and textural study of an LCT pegmatite: implications for the magmatic versus metasomatic origin of Nb-Ta mineralization in the Moose II pegmatite, Northwest Territories, Canada. *Journal of Geosciences*, (2013) 58, 299–320. [DOI:10.3190/jgeosci.149](https://doi.org/10.3190/jgeosci.149)
- [27] Van Lichtervelde, M., Holtz, F., Melcher, F., The effect of disequilibrium crystallization on Nb-Ta fractionation in pegmatites: Constraints from crystallization experiments of tantalite-tapiolite. *American Mineralogist*, (2018), 103(9), 1401-1416. <https://doi.org/10.2138/am-2018-6441>